Supplementary Information (SI) for Nanoscale.

Supplementary Information

Comprehensive Understanding of the Correlation between Structure and Harmonic Properties of Multicore Superparamagnetic Particles

Mari Takahashi,[1] Sakuya Shimizu,[1] Haruki Goto,[2] Satoshi Ota,[3] Takashi Yoshida,[4] and Shinya Maenosono[1,*]

1 *School of Materials Science, Japan Advanced Institute of Science and Technology, 1-1 Asahidai, Nomi, Ishikawa 923-1292, Japan*
2 *Department of Optoelectronics and Nanostructure Science, Graduate School of Science and Technology, Shizuoka University, Hamamatsu 432-8561, Japan*
3 *Department of Electrical and Electronic Engineering, Shizuoka University, Hamamatsu 432-8561, Japan*
4 *Department of Electrical Engineering, Kyusyu University, Fukuoka 819-0395, Japan*

*E-mail: shinya@jaist.ac.jp; +81-(0)761-51-1611

Table of Contents

1. Synthesis of Multicore Superparamagnetic Particles (MCPs)

The MCPs used in this study were synthesized by slightly modifying the solvothermal method reported previously.[1] The specific synthesis method is described below.

Chemicals and Equipment

Iron(III) chloride hexahydrate ($FeCl_3 \cdot 6H_2O$), urea, ethylene glycol (EG), polyacrylic acid (PAA) were purchased from Sigma-Aldrich. The average molecular weight of PAA is 2 kDa (catalog No. 323667). Pure water was produced using Direct-Q UV (Merk Millipore). A sample container for high pressure reaction made of polytetrafluoroethylene (PTFE) including carbon (HUTc-25) and an autoclave (HUS-25) were purchased from SAN-AI Kagaku Co., Ltd., Japan. For the heating reaction, a constant-temperature drying oven (EOP-300V, AS ONE Corporation, Japan) was used.

Sample Synthesis and Preparation Procedure

First, 3 mmol of $FeCl_3 \cdot 6H_2O$ and 20 mmol of urea were added to 20 mL of EG. They were stirred for 10 min at room temperature until the reagents dissolved completely. Then x mg of PAA and y mL of pure water were added to the mixture. The mixture was stirred for an additional 10 min at room temperature to completely dissolve the PAA. Subsequently, 17.5 mL of the solution mixture was transferred to the PTFE container. The container was placed in the autoclave and positioned in the center of the oven. Then, the oven temperature was raised to 250 °C, taking 80 min from room temperature (about 3 °C·min^{-1}). Upon reaching 250 °C, the temperature was maintained for 6 hours. After the reaction, the temperature was allowed to cool naturally inside the oven. After the temperature reached room temperature, the autoclave was taken out and the reaction mixture was divided into two centrifugation tubes. Pure water was added to each tube until the total volume became 40 mL. The reaction solution was sonicated to fully disperse the particles and the tubes were then centrifuged at speeds ranging from 500 to 5,000 g depending on MCP size. A low centrifugation speed (500 g) was used for large MCPs while a high speed (5,000 g) was used for small MCPs. After discarding the supernatant, the washing process was repeated twice using pure water.

Finally, 5 mL of pure water was added to one tube while the other tube was dried using a vacuum drying oven. The powder sample was analyzed using an X-ray diffractometer (XRD, Rigaku, MiniFlex600 with Cu Kα source). The solution sample was diluted for mounting on a Cu grid and observed using a transmission electron microscope (TEM, Hitachi, H-7650 operated at 100 kV). The mean crystalline size (D_{XRD}) was calculated by applying the Scherrer formula to the primary peak. The secondary particle size (D_{TEM}) was calculated as the average equivalent circular diameter using ImageJ software for approximately 30 to 60 randomly-selected secondary particles from the TEM images. Additionally, the diluted sample was analyzed by dynamic light scattering (Zetasizer Nano ZS, Malvern) to obtain the hydrodynamic size (D_{DLS}). The concentration of the MCP solutions were adjusted to 1.63 $mg_{Fe} \cdot mL^{-1}$ (the method is described below) and analyzed by an alternating current

susceptibility (ACS) measurement (100 μT, 10~10 kHz), magnetic particle spectroscopy (MPS) measurement[2] (20 mT, 1−30 kHz) and a magnetic relaxation (MR) measurement[3,4] (20 mT).

References

[1] Ganesan, V.; Lahiri, B. B.; Louis, C.; Philip, J.; Damodaran, S. P. Size-Controlled Synthesis of Superparamagnetic Magnetite Nanoclusters for Heat Generation in An Alternating Magnetic Field. *J. Mol. Liq.* **2019**, 281, 315–323.

[2] Sasayama, T.; Yoshida, T.; Tanabe, K.; Tsujimura, N.; Enpuku, K. Hysteresis Loss of Fractionated Magnetic Nanoparticles for Hyperthermia Application. *IEEE Trans. Magn.* **2015**, 51, 5101504.

[3] Ota, S.; Takemura, Y. Characterization of Néel and Brownian Relaxations Isolated from Complex Dynamics Influenced by Dipole Interactions in Magnetic Nanoparticles. *J. Phys. Chem. C* **2019**, 123 (47), 28859–28866.

[4] Goto, H.; Futagawa, M.; Takemura, Y.; Ota, S. Effects of Néel and Brownian Relaxations on Dynamic Magnetization Empirically Characterized in Single-Core and Multicore Structures of Magnetic Nanoparticles. *Nanoscale* **2025**, 17, 12817–12825.

Table S1 Synthesis conditions for the 14 types of MCPs investigated in this study.

Sample name	PAA (*x* mg)	Pure water (*y* mL)	Reaction temperature (°C)	Position in the oven
P2	100	2.0	210	Center
P3	100	1.5	210	Center
P4	150	2.25	210	Center
P5	100	1.7	250	Center
P6	250	3.0	210	Center
P7	150	2.0	210	Center
P8	200	1.0	250	Center
P9	150	1.75	210	Center
P10	250	2.5	210	Center
P11	200	1.5	250	Center
P12	250	2.5	250	Center
P13	400	2.5	250	Center
P14	300	2.75	250	Center
P15	100	1.5	250	Off-center (towards the wall)

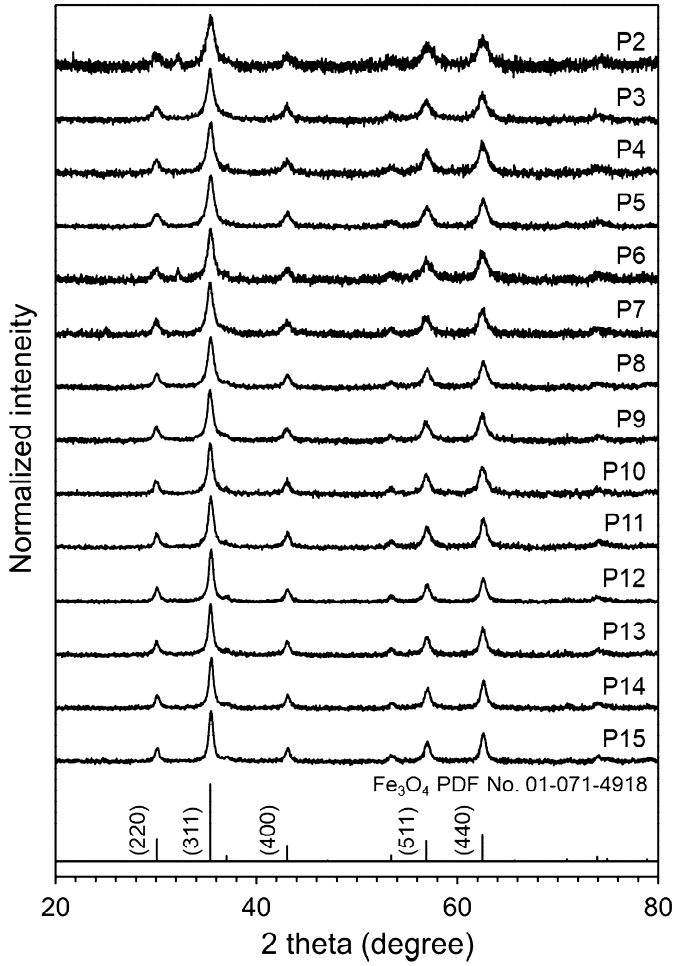

Fig. S1 XRD patterns of the 14 types of MCPs investigated in this study.

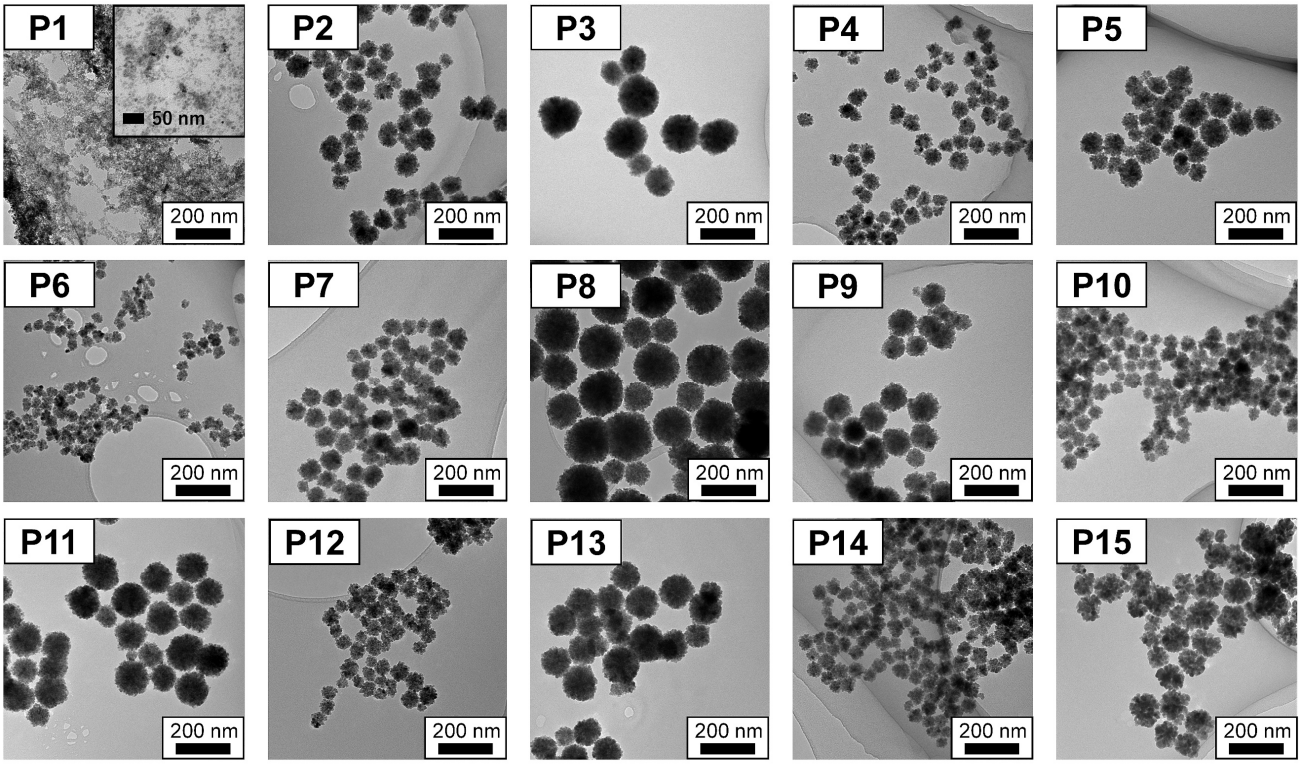

Fig. S2 TEM images of the 14 types of MCPs and Resovist® (**P1**) investigated in this study.

Table S2 Information on the sizes of the 14 types of MCPs investigated in this study.

Sample name	D_{XRD} (nm)	D_{TEM} (nm)	D_{DLS_n} (nm)	D_{DLS_i} (nm)	D_{ACS} (nm)
P2	9.5	86.8 ± 11.6	79	133	114
P3	10.1	135.3 ± 20.2	122	183	195
P4	10.9	70.8 ± 7.3	62	141	123
P5	11.2	101.0 ± 15.7	210	472	167
P6	11.8	49.2 ± 5.0	72	151	114
P7	11.8	82.5 ± 10.7	65	136	155
P8	12.1	169.3 ± 23.7	302	520	195
P9	12.8	102.2 ± 17.5	163	368	155
P10	13.6	65.4 ± 6.8	56	195	144
P11	13.6	122.1 ± 18.0	117	204	167
P12	16.1	65.8 ± 9.8	219	494	167
P13	16.1	120.3 ± 17.2	462	669	133
P14	16.8	62.4 ± 6.9	231	619	195
P15	17.4	118.6 ± 17.4	278	547	N/A

D_{DLS_n} and D_{DLS_i} are the mean hydrodynamic diameters calculated from the particle size distribution based on particle number (n) and scattered light intensity (i).

2. Formation Mechanism of MCPs (Effects of PAA and Water)

D_{XRD} and D_{TEM} can be controlled by varying the amounts of PAA and pure water. Here, we will examine the formation mechanism of the MCPs in detail. Based on a previous report,[1] during solvothermal reactions, urea [$CO(NH_2)_2$] decomposes into ammonia (NH_3) and isocyanic acid (HNCO) according to Eq. (S1). In the presence of trace amounts of water, HNCO reacts with water to produce NH_3 according to Eq. (S2). Urea also reacts with trace amounts of water to produce NH_3 according to Eq. (S3). NH_3 reacts with water according to equation (4) to form hydroxide ions.

$$CO(NH_2)_2 \rightarrow NH_3 + HNCO \quad \text{(S1)}$$

$$HNCO + H_2O \rightarrow NH_3 + CO_2 \quad \text{(S2)}$$

$$CO(NH_2)_2 + H_2O \rightarrow 2NH_3 + CO_2 \quad \text{(S3)}$$

$$NH_3 + H_2O \rightarrow NH_4^+ + OH^- \quad \text{(S4)}$$

On the other hand, EG undergoes deprotonation to generate acetaldehyde according to Eq. (S5). This acetaldehyde then reduces Fe^{3+} to Fe^{2+}.

$$2C_2H_6O_2 \rightarrow 2CH_3CHO + 2H_2O \quad \text{(S5)}$$

The iron ions react with hydroxide ions to form iron hydroxide species as in Eq. (S6). Finally, the iron hydroxide species are decomposed to form magnetite shown in Eq. (S7).

$$Fe^{2+} + 2Fe^{3+} + 8OH^- \rightarrow Fe^{II}Fe_2^{III}(OH)_8 \quad \text{(S6)}$$

$$Fe^{II}Fe_3^{III}(OH)_8 \rightarrow Fe^{II}Fe_2^{III}O_4 + 4H_2O \quad \text{(S7)}$$

One of the key roles of PAA is to function as a linker that connects primary particles to form stable MCPs.[2] In addition to this role, PAA is known to release protons at high pH (Eq. (S8)), and to form complexes with Fe ions (Eq. (S9)).[3,4]

$$PAA \rightarrow PAA^{n-} + nH^+ \quad \text{(S8)}$$

$$\alpha Fe^{2+} + \beta Fe^{3+} + PAA^{n-} \rightarrow Fe_{(\alpha+\beta)} - PAA\ (\text{chelate}) \quad \text{(S9)}$$

A closer examination of the contour plot of D_{XRD} (Figure 1a) reveals that, as briefly explained in the main text, the primary particle size increases with increasing water content in the region where the PAA amount (x) exceeds 150 mg. In this region, the large amount of water raised the pH of the reaction solution, generating more PAA anions according to Eq. (S8). Therefore, it is reasonable to conclude that complex formation between PAA anions and Fe ions was promoted according to Eq. (S9), suppressing the formation of iron hydroxide ($Fe^{II}Fe_2^{III}(OH)_8$). Due to the shortage of the iron hydroxide intermediate, $Fe^{II}Fe_2^{III}O_4$ crystal growth became dominant over nucleation. Consequently, when $x \geq 150$ mg, larger primary particles were obtained as the amount of pure water (y mL) increased. On the other hand, when $x < 150$ mg , the opposite trend was observed (Figure 1a). In this region, the chelating effect of PAA was reduced to the point of negligibility. Increasing y and the resulting pH increase merely helped intermediate formation according to Eq. (S6). Therefore, $Fe^{II}Fe_2^{III}O_4$ nucleation became dominant over crystal growth. As a result, smaller primary particles were obtained with increasing y. In other words, the intermediate formation and the complex formation are competing reactions, and which one becomes dominant is determined by the values of x and y.

As shown in Figure 1a and 1b, D_{XRD} tends to be smaller ($D_{XRD} < 11$ nm) when D_{TEM} is larger. This is because smaller primary particles have a higher surface energy and are more prone to agglomeration.[2] In the presence of a large amount of PAA, PAA also helped to link primary particles resulting in the formation of larger MCPs (depending on D_{XRD}). On the other hand, once the amount of PAA was decreased ($x < 300$ mg), it could not act as effective linker, and thus relatively smaller MCPs were formed. It should be noted that Figure 1a and 1b were derived from samples obtained at a reaction temperature of 250 °C. Judging from the two contour plots, it is evident that obtaining MCPs with smaller values for both D_{XRD} and D_{TEM} is difficult. Therefore, we fine-tuned D_{XRD} while maintaining D_{TEM} by changing the reaction temperature. Specifically, to reduce D_{XRD} while maintaining D_{TEM}, the reaction temperature was lowered to 210 °C. Conversely, to increase D_{XRD}

while maintaining D_{TEM}, the autoclave was positioned slightly off-center (toward the back wall) within the oven. This slightly raised the reaction temperature, enabling D_{XRD} to be increased by 2–7 nm, depending on the experimental conditions. This oven features a curved heating element beneath the shelf where the autoclave is installed. The curved section near the back wall causes temperatures in the vicinity of the wall to be higher than in the center (according to the specifications, a temperature gradient of approximately 30 °C was produced at a set temperature of 300 °C). Therefore, by positioning the autoclave slightly closer to the wall, it is possible to subtly increase the reaction temperature. This method provides excellent reproducibility. However, unfortunately, it was not possible to measure the precise temperature inside the autoclave.

References

[1] Su, M.; He, C.; Shih, K. Facile Synthesis of Morphology and Size-Controlled α-Fe_2O_3 And Fe_3O_4 Nano-And Microstructures by Hydrothermal/Solvothermal Process: The Roles of Reaction Medium and Urea Dose. *Ceram. Int.* **2016**, 42, 14793–14804.

[2] Ganesan, V.; Lahiri, B. B.; Louis, C.; Philip, J.; Damodaran, S. P. Size-Controlled Synthesis of Superparamagnetic Magnetite Nanoclusters for Heat Generation in An Alternating Magnetic Field. *J. Mol. Liq.* **2019**, 281, 315–323.

[3] Gao, X.; Yan, R.; Ma, H.; Song, L. Novel Preparation System of An Organic-Inorganic Hybrid Chemical Conversion Layer with High Chlorine Tolerance: A Characterization And Mechanism Study. *Surf. Coat. Technol.* **2020**, 392, 125739.

[4] Zhu, Y.; Sun, L.; Hou, M.; Yu, J.; Yu, C.; Zhang, Z.; Yang, H.; Liu, C.; Huang, L.; Jiang, D.; Zhang, Y.; Yuan, Y.; Zhu, X. An "Inside-Out"-Guided Genetically Engineered Hydrogel for Augmenting Aged Bone Regeneration. *Bioact. Mater.* **2025**, 51, 318–332.

3. Concentration Adjustment Method

To accurately adjust the concentration of the MCPs, a calibration curve was created. The specific procedure is outlined below. First, MCPs dispersed in water at different concentrations were prepared, and their absorption spectra were obtained using a JASCO V-750 spectrophotometer. The solid content in the MCP dispersion was confirmed by freeze-drying the dispersion whose absorption spectrum was measured, then weighing the residue. The absorbance at a wavelength of 500 nm (OD_{500}) was measured for each concentration. Figure S3a shows the OD_{500} values for each MCP dispersion concentration and the approximate straight line (calibration curve passing through the origin). Using this calibration curve (OD_{500}=16.07C), the concentration of all MCPs was adjusted to 2.5 mg·mL^{-1} for ACS, MPS, and MR measurements.

Next, to quantify the PAA content in the MCPs, thermogravimetric analysis (TGA; Mettler Toledo TGA/SDTA851) was performed in air on **P8**, **P12**, and **P13**, which have different D_{XRD} and D_{TEM} values. Figure S3b shows the mass loss curve for **P13** as a representative example (similar mass loss curves were obtained for **P8** and **P12**). Note that TGA measurement of PAA alone confirmed its complete decomposition and volatilization at approximately 570 °C. After TGA measurement, a phase

transition from Fe_3O_4 to α-Fe_2O_3 (hematite) was observed, as shown in Figure S3c. The oxidation of Fe_3O_4 proceeded according to the following chemical equation:

$$4Fe_3O_4 + O_2 \rightarrow 6Fe_2O_3 \quad \text{(S10)}$$

Based on Eq. (S10), the percentage of mass increase (Δm) was calculated by the following equation (Eq. (S11)) using the atomic weights of Fe and O.

$$\Delta m = \frac{O_2}{4Fe_3O_4} \times 100 = 3.46\ (\%) \quad \text{(S11)}$$

Assuming the initial masses of Fe_3O_4 and PAA are p mg and q mg, respectively, the final mass (hematite mass) is $1.0346p$ mg according to Eq. (S11). Since the initial mass $(p + q)$ and final mass $(1.0346p)$ of the sample are known, solving the simultaneous equations yields p and q. The initial mass (m_i), final mass (m_f), p and q are summarized in Table S3. The results clearly show that regardless of the MCP morphology, the weight ratio of Fe_3O_4:PAA is always 9:1. Therefore, according to Eq. (S12), a concentration of 2.5 mg·mL^{-1} of MCPs corresponds to 1.63 mg_{Fe}·mL^{-1}.

$$2.5\ (mg \cdot mL^{-1}) \times 0.9 \times \frac{3Fe}{Fe_3O_4} = 1.63\ (mg_{Fe} \cdot mL^{-1}) \quad \text{(S12)}$$

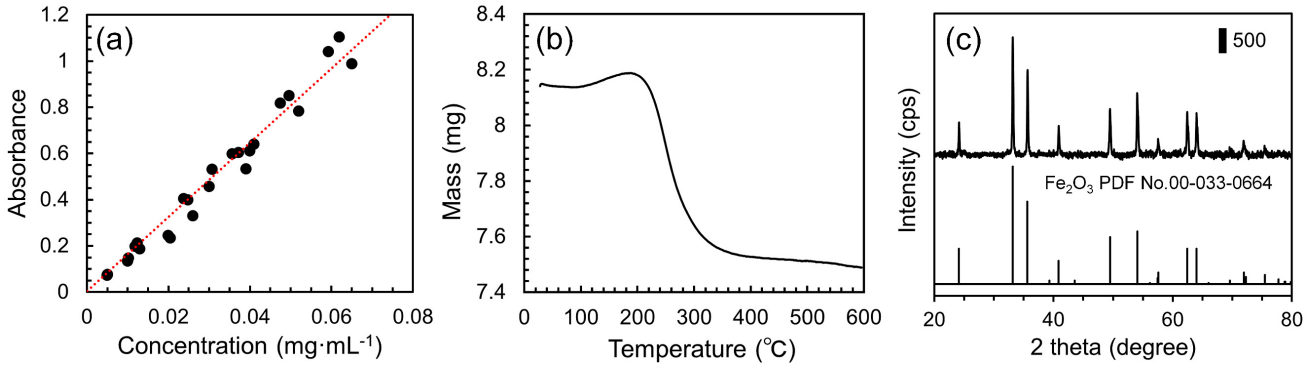

Fig. S3 (a) Calibration curve (red dashed line) for concentration measurement. (b) TGA result and (c) XRD pattern after TGA measurement for **P13** as an example.

Table S3 Each weight determined through TGA.

Sample name	m_i (mg)	m_f (mg)	p (mg)	q (mg)
P8	7.65	6.99	6.75	0.90
P12	8.27	7.67	7.42	0.85
P13	8.14	7.49	7.24	0.90

4. Experimental Setup and Results for MPS Measurements

MPS Measurement

The AC *M–H* curve of the sample was measured using a homemade MPS system.[1] A resonant circuit with a variable capacitor was used to apply an AC excitation field. The capacitance of the variable capacitor was set so that its resonant frequency matches the excitation frequency, f. The AC excitation field, $H(t) = H_0 \cos(2\pi f t)$, was applied via a solenoidal coil. The excitation coil, which contains 96 turns, is made from a Litz wire with 2000 0.04-mm-diameter filaments. In this MPS setup, H_0 and f can be adjusted up to 30 mT/μ_0 and 30 kHz, respectively. The detection and cancellation coils, each of which has 44 turns, are made from a single wire (0.2mm diameter).

The voltage, $v_\mathrm{s}(t)$, across the shunt resistance and the difference voltage, $v_\mathrm{m}(t)$, between the detection and cancellation coils were measured using an A/D converter (National Instruments Corporation, PXIe-5122, 14 bit, 100 MS/s) and the voltage data were averaged 1000 times to reduce the noise floor. The AC excitation field, $H(t)$, was obtained from the measured $v_\mathrm{s}(t)$. According to Faraday's law, the relationship between $v_\mathrm{m}(t)$ and the mass magnetization, $M(t)$, of the sample, i.e., the magnetic moment in the direction of excitation field per unit iron mass, is given by

$$v_\mathrm{m}(t) = \frac{\mathrm{d}M(t)}{\mathrm{d}t} \times \frac{m_\mathrm{Fe}}{V_\mathrm{sample}} \int_\Omega s(\boldsymbol{r})\mathrm{d}\boldsymbol{r} \qquad \text{(S13)}$$

Here, V_sample and m_Fe are the sample volume and the amount of iron used, respectively. Ω denotes the three-dimensional region containing the sample, $s(\boldsymbol{r})$ denotes the sensitivity profile of the detection coil, and $\int_\Omega s(\boldsymbol{r})\mathrm{d}\boldsymbol{r}$ of the MPS system was experimentally derived from a standard sample with known magnetization and $v_\mathrm{m}(t)$. From Eq. (S13), $M(t)$ was obtained by the integral over time of $v_\mathrm{m}(t)$ and the amplitudes of the harmonic magnetization, i.e., the MPS spectra, were obtained from the amplitudes of the Fourier transformation of $M(t)$.

References

[1] Sasayama, T.; Yoshida, T.; Tanabe, K.; Tsujimura, N.; Enpuku, K. Hysteresis Loss of Fractionated Magnetic Nanoparticles for Hyperthermia Application. *IEEE Trans. Magn.* **2015**, 51, 5101504.

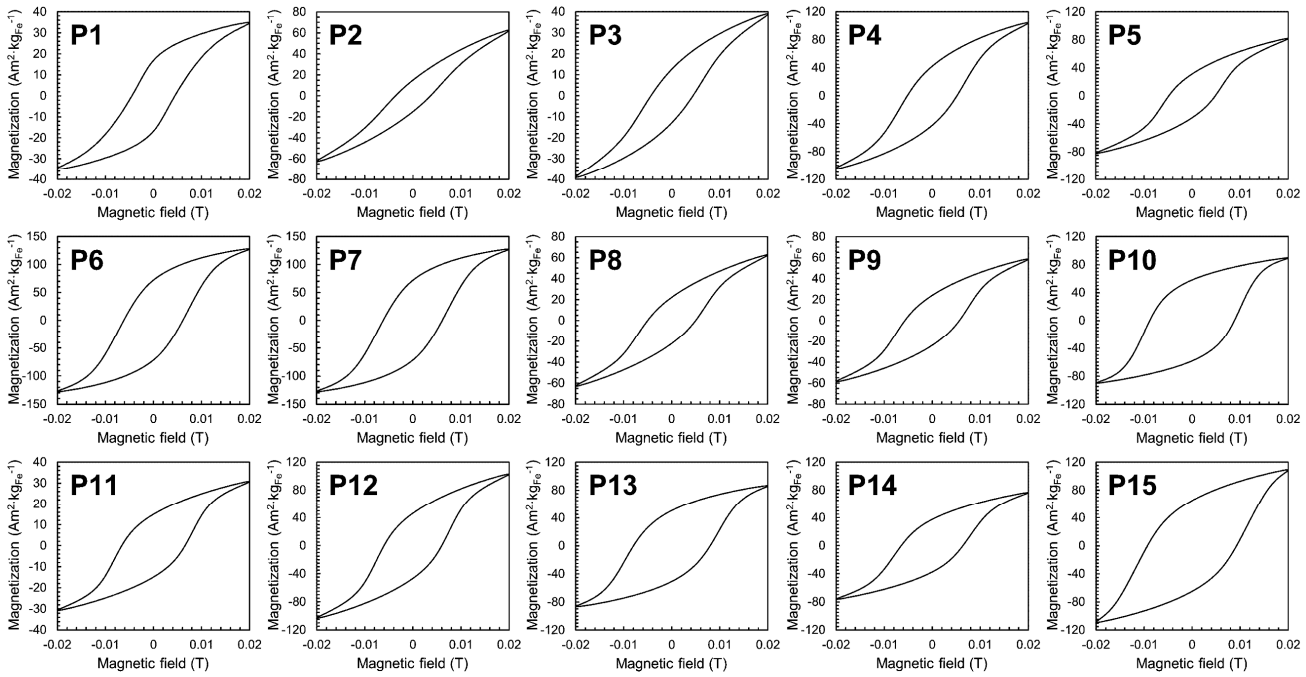

Fig. S4 Magnetization curves obtained for the 14 types of MCPs and Resovist® (**P1**) via MPS measurement (20 kHz, 20 mT).

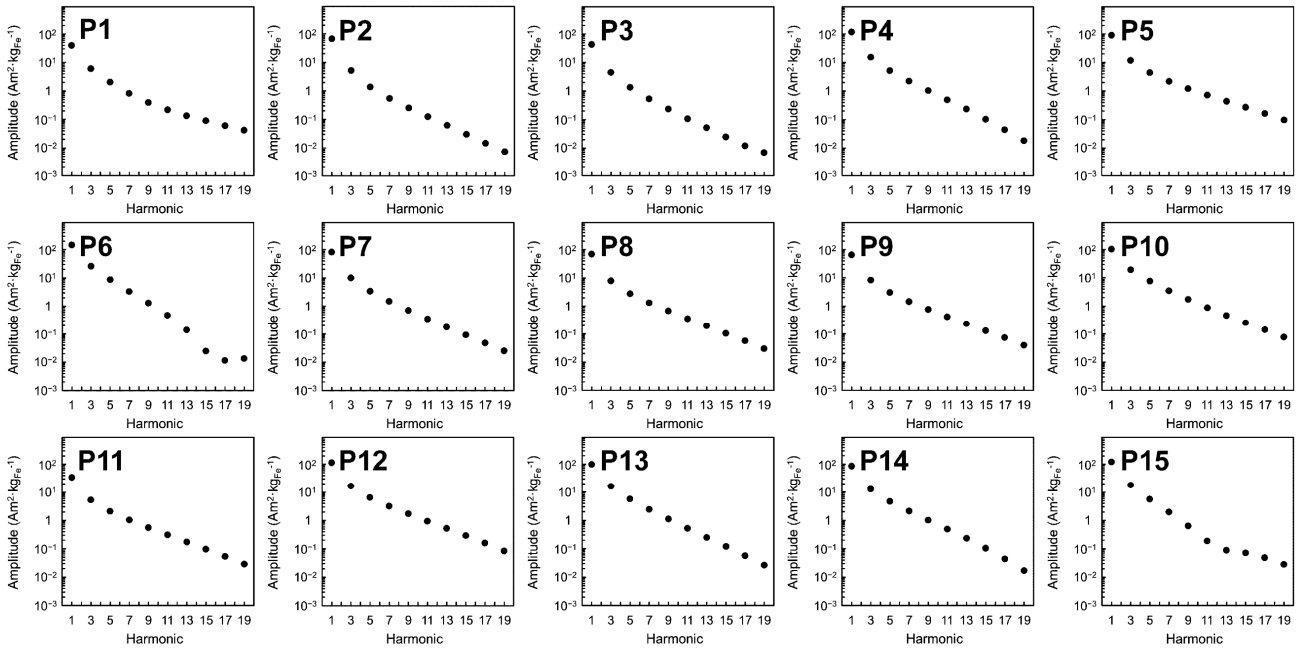

Fig. S5 MPS spectra of the 14 types of MCPs and Resovist® (**P1**) via MPS measurement (20 kHz, 20 mT).

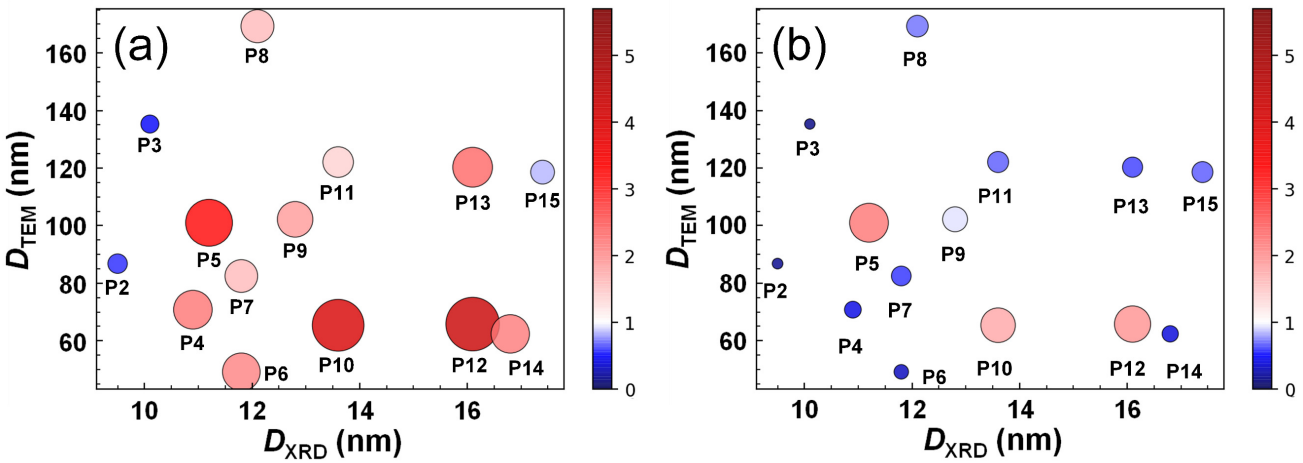

Fig. S6 Bubble plots of (a) I_{11} (the eleventh harmonic intensity) and (b) I_{19} (the nineteenth harmonic intensity) in a D_{XRD}-D_{TEM} coordinate space. The harmonic intensities of **P2**–**P15** were normalized using the value of the same harmonic intensity of **P1** (Resovist®). Red and blue colors indicate $I_i > 1$ and $I_i < 1$, respectively ($i = 11$ or 19).

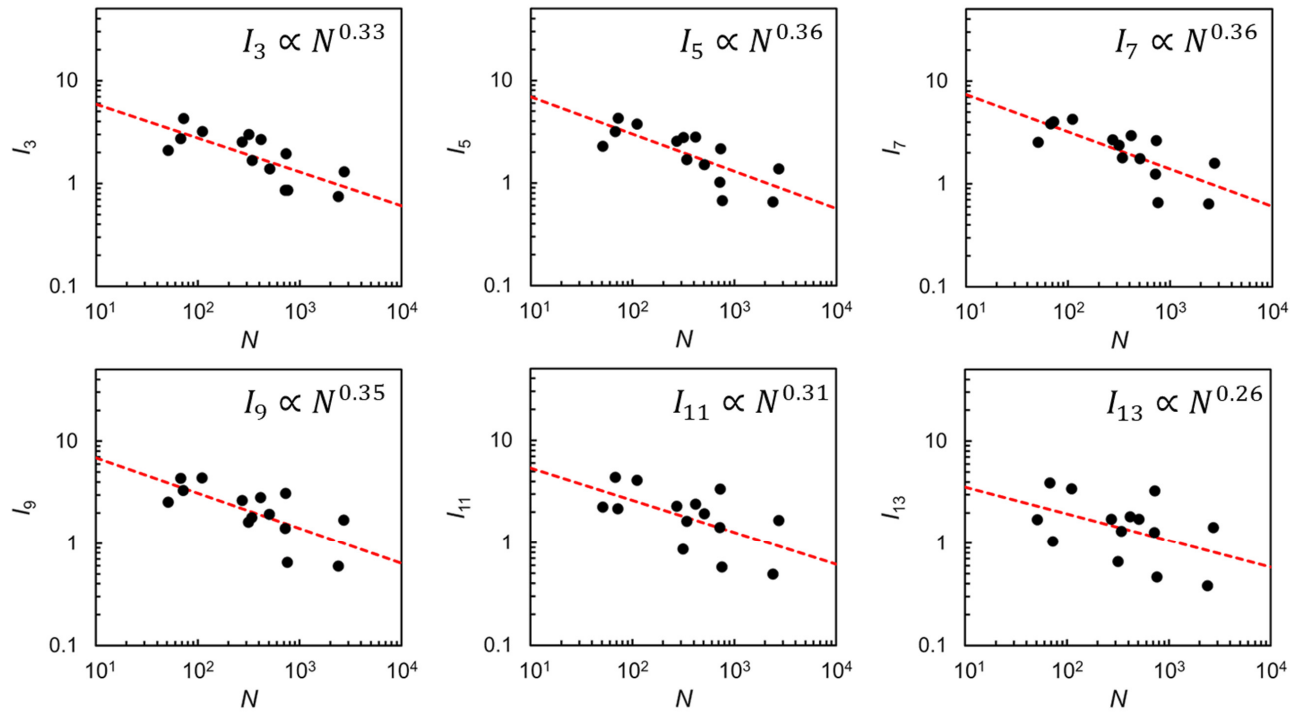

Fig. S7 Correlation between higher harmonics (from third to thirteenth) and N.

Table S4. The number of primary particles constituting a single MCP (N).

Sample name	P2	P3	P4	P5	P6	P7	P8	P9	P10	P11	P12	P13	P14	P15
N	763	2404	274	733	72	342	2739	509	111	724	68	417	51	317

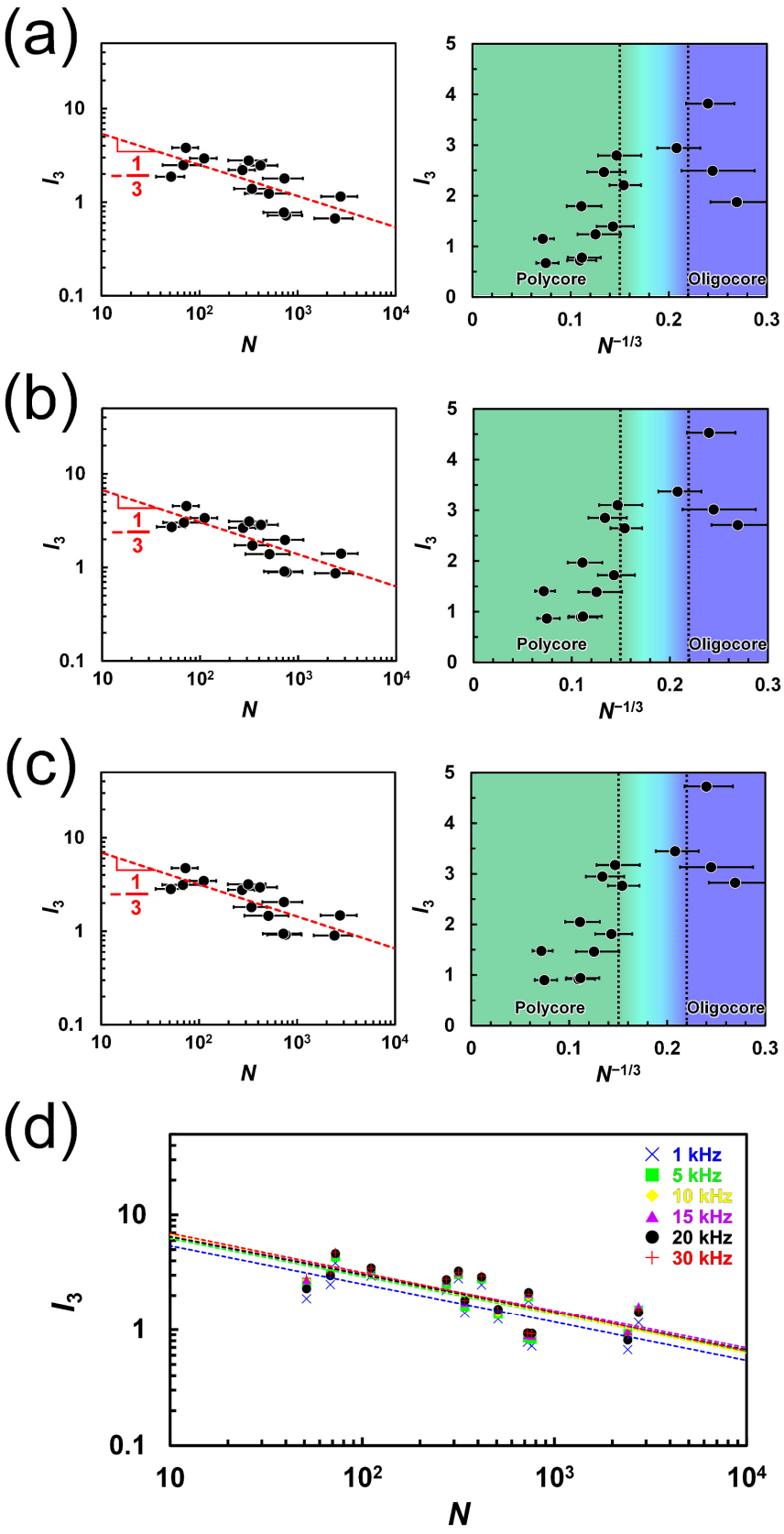

Fig. S8 (a-c) Log-log plot of I_3 versus N (left panel) and correlation between I_3 and $N^{-1/3}$ (right panel). Panels (a), (b), and (c) correspond to the results for AC magnetic field frequencies of 1 kHz, 10 kHz, and 30 kHz respectively (all with a magnetic field strength of 20 mT). (d) Log-log plot of I_3 versus N for all AC magnetic field frequencies (1 to 30 kHz).

5. Experimental Setup and Results for ACS and Magnetic Relaxation Measurements

ACS Measurement

The AC susceptibility (ACS) spectrum of the sample was measured using a homemade ACS system shown in Fig. S9. The AC excitation field, $H(t) = H_0 \cos(2\pi f t)$, was applied via a solenoidal coil. The excitation coil, which has 33 turns, is made from a single wire (0.8 mm diameter). In the ACS setup, H_0 is fixed at 100 μT/μ_0 and f ranges from 10 Hz to 10 kHz. The detection and cancellation coils, each of which has 100 turns, were made from a single wire (0.2 mm diameter).

The voltage, $v_s(t)$, across the shunt resistance and the difference voltage, $v_m(t)$, between the detection and cancellation coils at a fixed f were measured using a gain-phase analyzer (NF, ZGA5920) and the in-phase (real part), $V_R(f)$, and out-of-phase (imaginary part), $V_I(f)$, components of $v_m(t)$ with respect to $v_s(t)$ were obtained from the gain-phase analyzer. Since $v_m(t)$ is the induced voltage caused by the temporal change of the magnetization of sample and $v_s(t)$ is proportional to $H(t)$, the real, $\chi_R(f)$, and imaginary, $\chi_I(f)$, parts of the ACS measurement were calculated as $\chi_R(f) = kV_I(f)/f$ and $\chi_I(f) = -kV_R(f)/f$. Here, k is constant. By sweeping f an ACS spectrum, *i.e.*, spectra of $\chi_R(f)$ and $\chi_I(f)$, was finally obtained (Fig. S10).

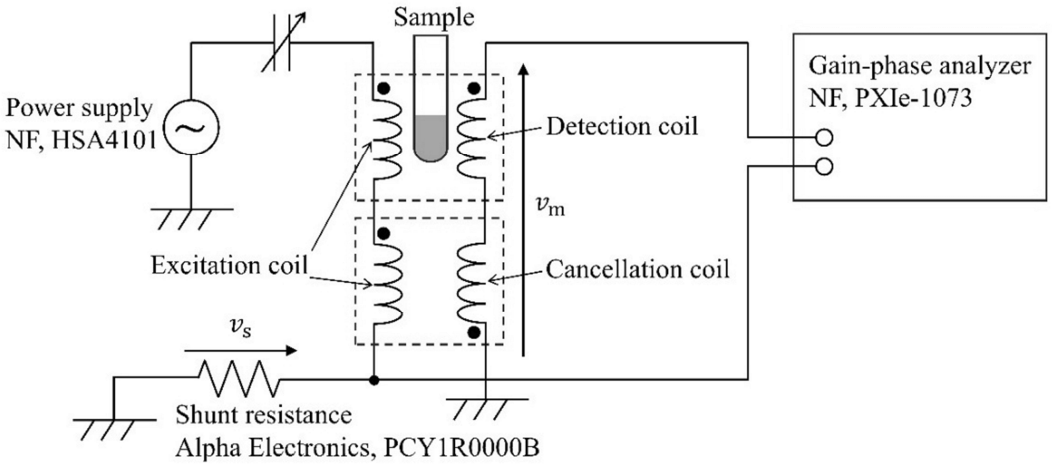

Fig. S9 ACS system.

Magnetic Relaxation Measurement and Analysis of Magnetic Relaxation Time

The magnetic relaxation process was measured using the measurement circuits shown in Fig. S11. The fast, middle, and slow responses of magnetic relaxation were measured by circuits (a), (b), and (c), respectively. To detect the fast response, the inductance of the excitation coil L_{ex} and detection coil L_{de} were small, and the cut-off frequency of the low pass filter, f_C, was high for the short time constant of the circuit. To detect the slow response, L_{ex} and L_{de} were large for high sensitivity, and f_C was low for the large attenuation of random noise.[1]

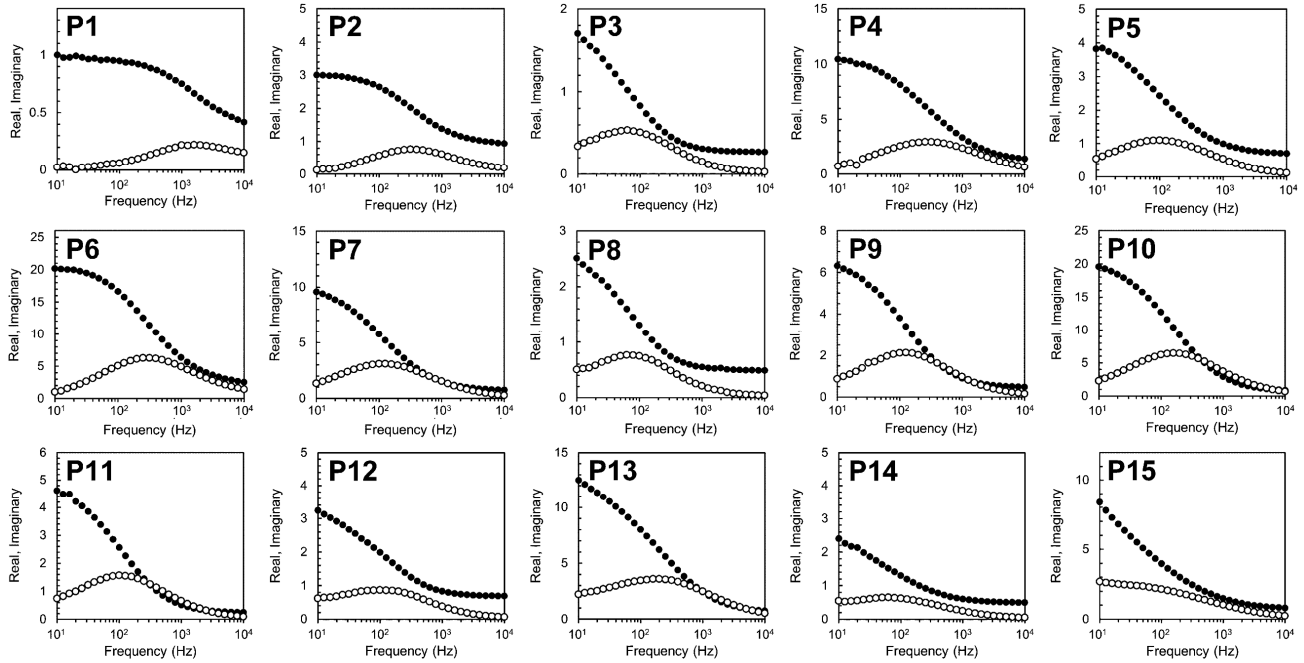

Fig. S10 ACS spectra of the 14 types of MCPs and Resovist® (**P1**) investigated in this study. Filled and open circles represent the real and imaginary parts of the magnetic susceptibilities, respectively. $\tau_{\mathrm{B,ACS}}$ was obtained based on the peak position of the imaginary part and is shown in Table S7.

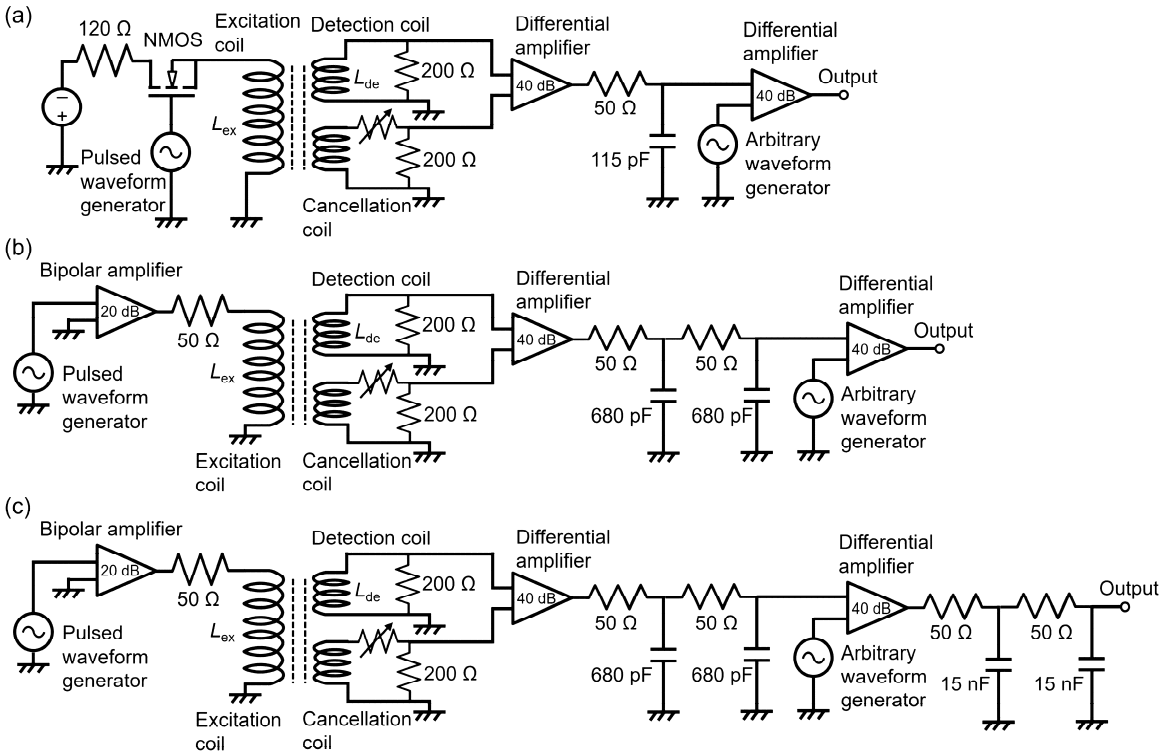

Fig. S11 Measurement circuits (a), (b), and (c) for the magnetic relaxation process in the fast, middle, and slow time range, respectively.

In circuit (a), the pulsed current was applied to the excitation coil by the direct current (DC) power supply (CM250-9; NF Corporation, Yokohama, Japan). The current was switched by the n-type MOSFET controlled by a function generator (WF1984; NF Corporation, Yokohama, Japan). In circuits (b) and (c), the pulse current was generated by a bipolar power supply (HSA4014; NF Corporation, Yokohama, Japan) and controlled by the function generator.

The magnetization signal was detected by the induced voltage according to Faraday's law. In all detection circuits, the voltage derived from the applied magnetic field was reduced by the cancellation coil with the differential amplifier SA-440F5 driven by the DC voltage source LP5392 (NF Corporation, Yokohama, Japan). The signal output from the first set of differential amplifier and low pass filter composed of the resistance and capacitance was stored and then generated as the arbitrary waveform from the function generator to additionally reduce the background signal derived from the applied magnetic field. In circuit-(c) only, the low pass filter of f_C = 1 MHz built into the differential amplifier was used. The output waveform was measured using an oscilloscope (MSO64 6-BW-1000; Tektronix Inc., Beaverton, OR, USA). The rise time of the pulsed waveform generator similar to that of the applied magnetic field, t_{rise}, and L_{ex} and L_{de} are shown in Table S5.

The distribution of the magnetic relaxation time τ was analyzed from the measured magnetic relaxation process using a machine learning approach.[1] The neural network in the deep learning framework was trained by the distribution of τ calculated based on the Gaussian distribution, A_{M}, as the output data and the magnetic relaxation process calculated from the prepared distribution of τ, M_{cal}, using Eq. (S14) as the input data.

$$M_{\mathrm{cal}}(t) = \sum_{i=1}^{N_\tau} A_{\mathrm{M},i} \left\{1 - \exp\left(-\frac{t}{\tau_i}\right)\right\} \quad \text{(S14)}$$

where N_τ is the number of points in A_{M} whose sum equals 1, t is the time.

Table S5 t_{rise}, L_{ex} and L_{de} in circuits (a),(b), and (c) shown in Fig. S11.

Circuit	**(a)**	**(b)**	**(c)**
t_{rise} (μs)	0.217	1.0	40
L_{ex} (μH)	0.456	11.0	45.1
L_{de} (μH)	0.0638	0.801	12.8

Attribution of Multiple Relaxation Time Peaks

Figure S12 shows the step response of magnetization for 9 MCPs under applied pulsed magnetic fields. By analyzing these magnetic responses, as described in the previous subsection, relaxation time

distributions were obtained (Figure S13). Clear peaks appearing after 1 μs are summarized in Table S6. To attribute these peaks, Brownian and Néel relaxation times were calculated using different sizes obtained from TEM, DLS, and ACS (Eqs. (S15)-(S22)) and summarized in Table S7. As evident from the TEM images (Figures S2) and size histogram (Figure S14), in several samples (**P9**, **P11** and **P13**), smaller MCPs were observed, and the size distribution exhibited a bimodal (or multimodal) shape. Assuming a bimodal distribution for simplicity and considering that the presence of these smaller MCPs ($D_{\mathrm{TEM\_small}}$) affects the relaxation time, the Brownian relaxation time was also calculated for the smaller MCPs.

$$\tau_{\mathrm{B,TEM\_small}} = \frac{3\eta V_{\mathrm{TEM\_small}}}{k_{\mathrm{B}}T} \quad \text{(S15)}$$

$$\tau_{\mathrm{B,TEM}} = \frac{3\eta V_{\mathrm{TEM}}}{k_{\mathrm{B}}T} \quad \text{(S16)}$$

$$\tau_{\mathrm{B,DLS\_n}} = \frac{3\eta V_{\mathrm{DLS\_n}}}{k_{\mathrm{B}}T} \quad \text{(S17)}$$

$$\tau_{\mathrm{B,DLS\_i}} = \frac{3\eta V_{\mathrm{DLS\_i}}}{k_{\mathrm{B}}T} \quad \text{(S18)}$$

$$\tau_{\mathrm{B,ACS}} = \frac{3\eta V_{\mathrm{ACS}}}{k_{\mathrm{B}}T} \quad \text{(S19)}$$

$$\tau_{\mathrm{N,XRD}} = \tau_0 \exp\left(\frac{KV_{\mathrm{XRD}}}{k_{\mathrm{B}}T}\right) \quad \text{(S20)}$$

$$\tau_{\mathrm{N,TEM\_small}} = 6.373 \exp\left(1.932 \times 10^{-6} \times V_{\mathrm{TEM\_small}}\right) \quad \text{(S21)}$$

$$\tau_{\mathrm{N,TEM}} = \tau_{\mathrm{mid}} = 6.373 \exp\left(1.932 \times 10^{-6} \times V_{\mathrm{TEM}}\right) \quad \text{(S22)}$$

The subscripts beneath the volume V, τ_{B} and τ_{N} denote which measurement method yielded the particle size used; "small" indicates that the particle size of smaller MCPs observed in TEM images was employed. η of water at 25 °C is 0.00089 Pa·s.[2]

References

[1] Goto, H.; Futagawa, M.; Takemura, Y.; Ota, S. Effects of Néel and Brownian Relaxations on Dynamic Magnetization Empirically Characterized in Single-Core and Multicore Structures of Magnetic Nanoparticles. *Nanoscale* **2025**, 17, 12817–12825.

[2] W. M. Haynes, *CRC Handbook of Chemistry and Physics, 92nd ed.* Boca Raton, FL: CRC Press, 2011.

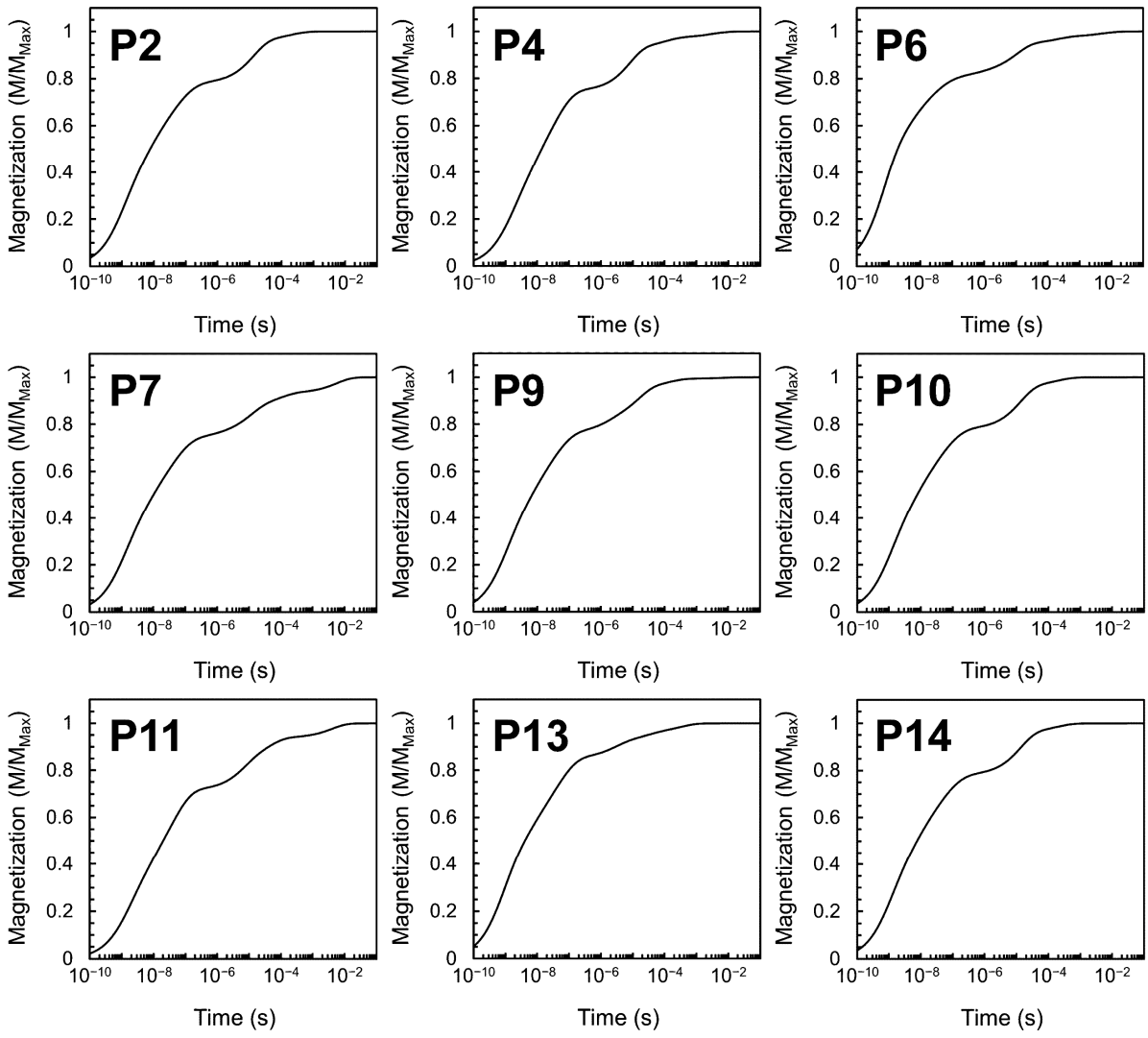

Fig. S12 Step responses of magnetization for 9 MCPs under applied pulsed magnetic fields.

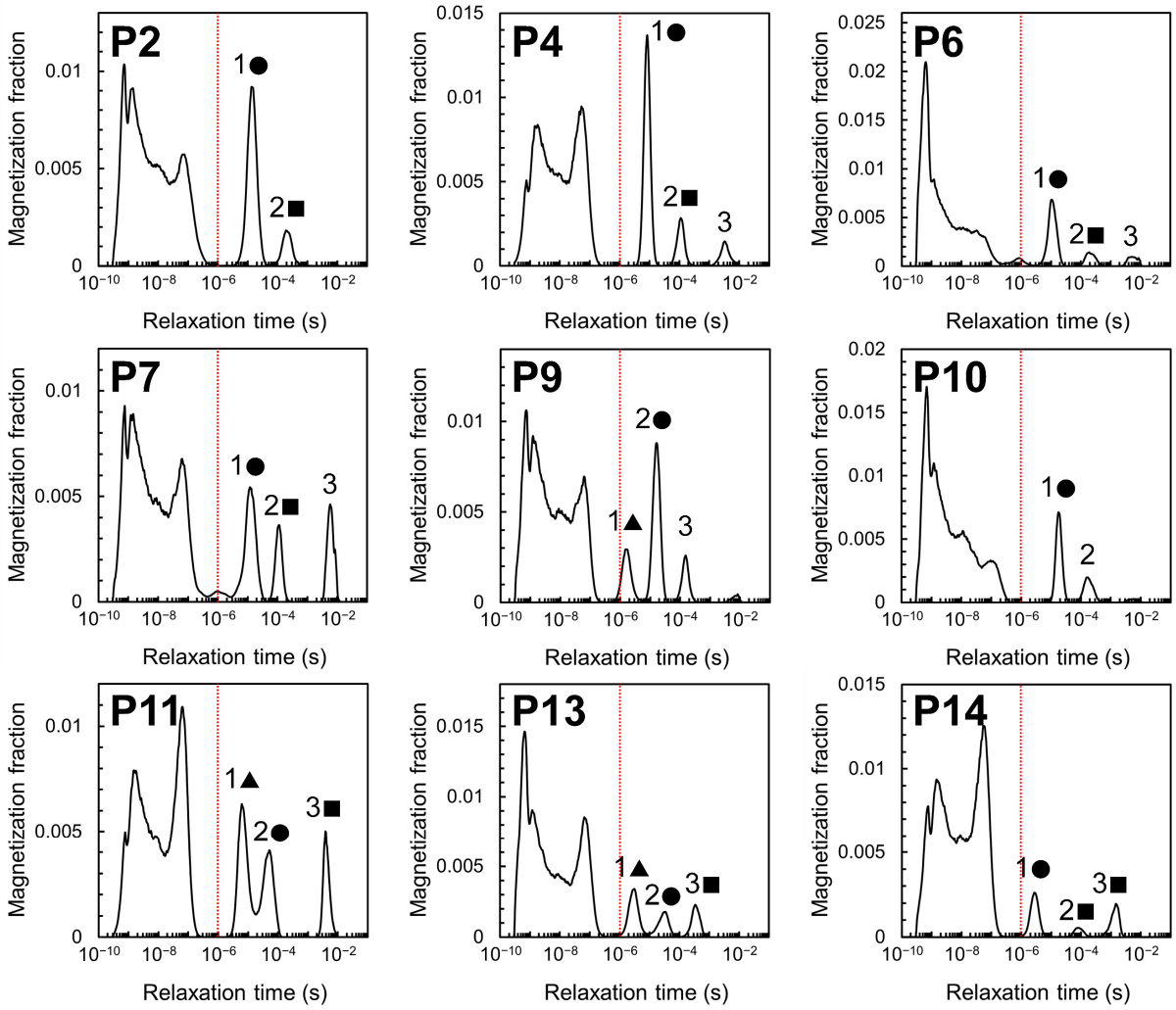

Fig. S13 Relaxation time distribution for 9 MCPs. ▲ indicates $\tau_{\mathrm{N,TEM\_small}}$, ● indicates $\tau_{\mathrm{N,TEM}}$, corresponding to τ_{mid} in the main text and ■ indicates τ_{B}. Note that τ_{B} covers both τ_{B} derived from smaller-sized and average-sized MCPs. The red dashed line represents the 1 μs line; the large peak to the left of this line corresponds to the fast Néel relaxation time of primary particles (in an isolated state). The unassigned, significantly long relaxation time peak corresponds to the Brownian relaxation time of some MCP aggregates that formed during measurement. For reference, if we treat the MCP as a single particle and calculate τ_{N} using $\tau_{\mathrm{N}} = \tau_0 \exp(KV_{\mathrm{TEM}}/k_{\mathrm{B}}T)$, we obtain astronomically large values (even for **P6** with the smallest V_{TEM}, it reaches the order of 10^{50} s). For **P11** and **P13**, the intensity of the peak considered to be the relaxation time of the smaller MCPs (▲) is equivalent to or greater than that of the peak marked with ●. This suggests the potential existence of numerous MCPs with particle sizes smaller than the average size determined from the TEM images. In other words, while the particle size distribution shown in Figure S14 indicates a few small particles, the actual number of smaller particles may be significantly higher (TEM images represent only a subset of particles and may not reflect the entire population).

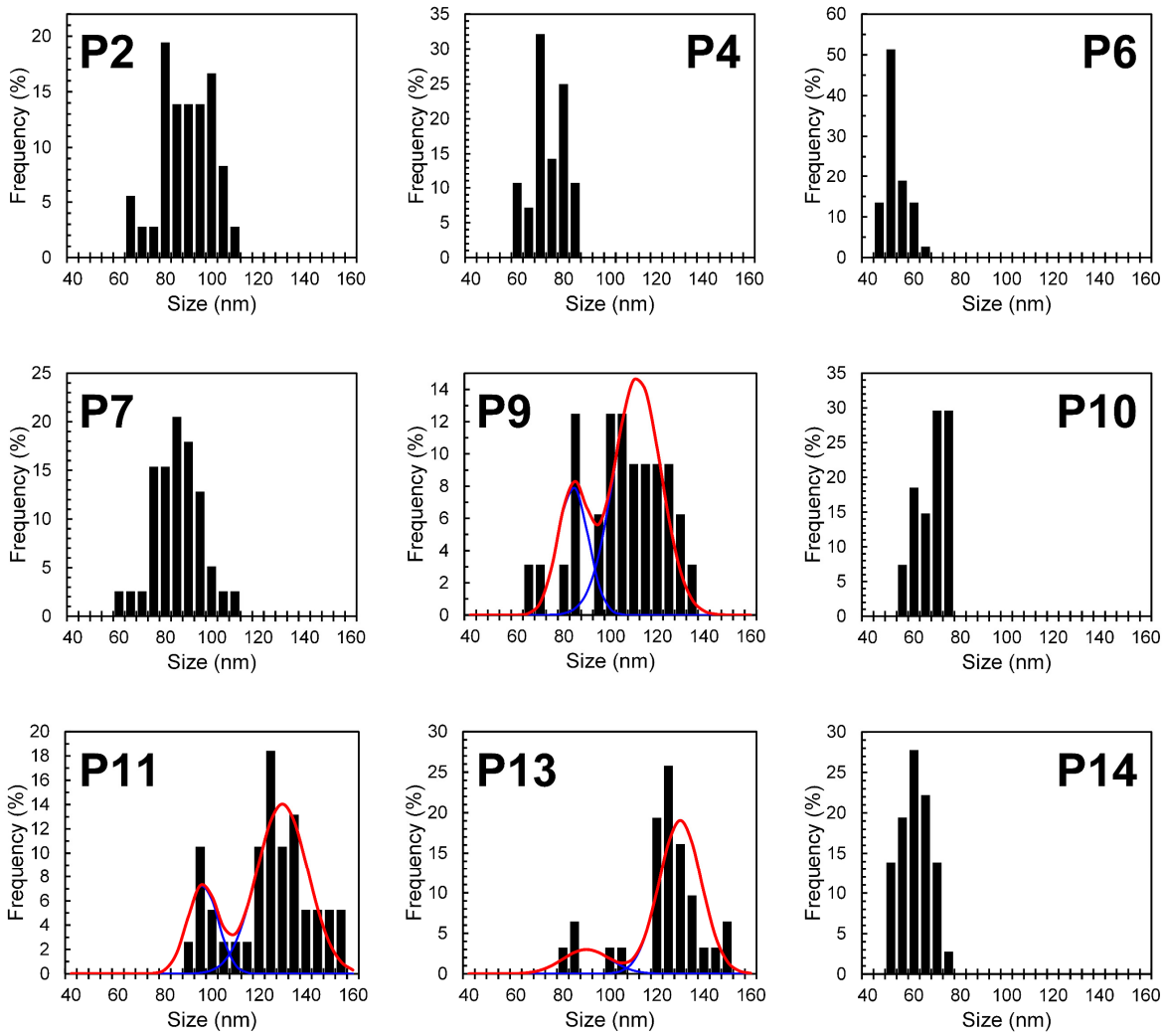

Fig. S14 Size distributions of 9 MCPs. The red curves plotted on the histograms for **P9**, **P11**, and **P13** are particle size distribution curves obtained by assuming a bimodal distribution and fitting with two Gaussian functions.

Table S6 Significant relaxation times exceeding 1 μs.

Sample name	Peak 1 (μs)		Peak 2 (μs)		Peak 3 (μs)	
P2	13.8	(●)	190.5	(■)	–	
P4	8.3	(●)	109.6	(■)	3311.3	(**UNASGD**)
P6	10.5	(●)	190.5	(■)	5248.1	(**UNASGD**)
P7	12.0	(●)	109.6	(■)	5754.4	(**UNASGD**)
P9	1.5	(▲)	15.8	(●)	151.4	(**UNASGD**)
P10	17.4	(●)	166.0	(**UNASGD**)	–	
P11	6.0	(▲)	50.1	(●)	3801.9	(■)
P13	3.2	(▲)	31.6	(●)	346.7	(■)
P14	2.8	(●)	83.2	(■)	1445.4	(■)

▲, ●, and ■ correspond to assignments to $\tau_{\mathrm{N,TEM\_small}}$, $\tau_{\mathrm{N,TEM}}$ (corresponding to τ_{mid} in the main text), and τ_{B}, respectively. UNASGD refers to unassigned peaks.

Table S7 Relaxation times calculated using Eqs. (S15) to (S22).

Sample name	$D_{\mathrm{TEM\_small}}$ (nm)	$\tau_{\mathrm{B,TEM\_small}}$ (μs)	$\tau_{\mathrm{B,TEM}}$ (μs)	$\tau_{\mathrm{B,DLS\_n}}$ (μs)	$\tau_{\mathrm{B,DLS\_i}}$ (μs)	$\tau_{\mathrm{B,ACS}}$ (μs)	$\tau_{\mathrm{N,XRD}}$ (μs)	$\tau_{\mathrm{N,TEM\_small}}$ (μs)	$\tau_{\mathrm{N,TEM}}$ (μs)
P2	–	–	222.2	166.3	801.2	503.4	0.003	–	12.3
P4	–	–	120.6	80.6	949.8	632.3	0.004	–	9.1
P6	–	–	40.5	125.1	1170	503.4	0.007	–	7.2
P7	–	–	190.8	93.3	859.8	1265	0.007	–	11.2
P9	84.0	201.4	362.7	1472	16883	1265	0.011	11.6	18.8
P10	–	–	95.0	59.5	2509	1015	0.018	–	8.5
P11	96.1	301.6	618.5	541.9	2903	1583	0.018	15.6	40.2
P13	90.0	247.7	591.6	33507	101891	799.4	0.119	13.3	37.1
P14	–	–	82.6	4172	80551	2520	0.228	–	8.1

$\tau_{\mathrm{N,TEM}}$ is calculated according to Eq. (S22) and it corresponds to experimentally measured τ_{mid} (see Fig. 3a). This calculated τ_{mid} $(= \tau_{\mathrm{N,TEM}})$ will henceforth be denoted as $\tau_{\mathrm{mid\_cal}}$.

Table S8 Summary of τ_{mid}, E_{C} and magnetic moments of MCPs.

Sample name	$\tau_{\mathrm{mid\_exp}}$ (μs)	$\tau_{\mathrm{mid\_cal}}$ (μs)	E_{C} ($\times 10^{-19}$ J)	μ ($\times 10^{-19}$ A·m^2)	$N\mu$ ($\times 10^{-17}$ A·m^2)	m ($\times 10^{-17}$ A·m^2)
P2	13.8	12.3	0.956	1.42	10.8	8.0
P3	N/A	78.1	1.032	1.19	28.5	19.0
P4	8.3	9.1	0.944	2.23	6.1	7.3
P5	N/A	18.1	0.972	1.83	13.4	16.6
P6	10.5	7.2	0.934	3.47	2.5	3.0
P7	12.0	11.2	0.952	2.37	8.1	8.3
P8	N/A	863.4	1.131	1.53	41.9	60.0
P9	15.8	18.8	0.973	2.42	12.3	12.3
P10	17.4	8.5	0.941	3.82	4.3	4.9
P11	50.1	40.2	1.005	2.44	17.7	11.0
P12	N/A	8.5	0.941	5.43	3.7	5.8
P13	31.6	37.1	1.001	3.52	14.7	29.6
P14	2.8	8.1	0.939	6.15	3.2	3.7
P15	N/A	34.5	0.998	4.16	13.2	35.8

$\tau_{\mathrm{mid\_exp}}$ and $\tau_{\mathrm{mid\_cal}}$ represent the experimentally obtained relaxation time and the relaxation time calculated by Eq. (S22) (see Fig. 3a), respectively.

6. Relationships between E_C and N, and I_3 and M_{max}

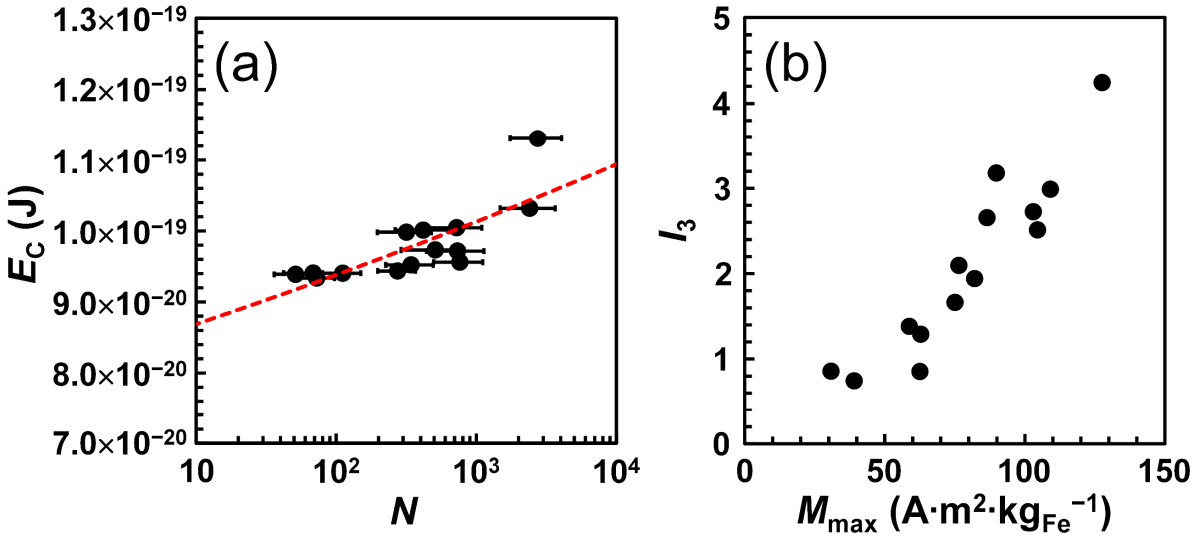

Fig. S15 (a) Semi-log plot of E_C versus N. (b) Correlation between I_3 and M_{max} (maximum magnetization in MPS measurement).